JVI Journals.ASM.org

Novel Functions of Hendra Virus G N-Glycans and Comparisons to Nipah Virus

Birgit G. Bradel-Tretheway,[a] Qian Liu,[a] Jacquelyn A. Stone,[a] Samantha McInally,[a] Hector C. Aguilar[a,b]

Paul G. Allen School for Global Animal Health[a] and Department of Veterinary Microbiology and Pathology,[b] Washington State University, Pullman, Washington, USA

ABSTRACT

Hendra virus (HeV) and Nipah virus (NiV) are reportedly the most deadly pathogens within the *Paramyxoviridae* family. These two viruses bind the cellular entry receptors ephrin B2 and/or ephrin B3 via the viral attachment glycoprotein G, and the concerted efforts of G and the viral fusion glycoprotein F result in membrane fusion. Membrane fusion is essential for viral entry into host cells and for cell-cell fusion, a hallmark of the disease pathobiology. HeV G is heavily N-glycosylated, but the functions of the N-glycans remain unknown. We disrupted eight predicted N-glycosylation sites in HeV G by conservative mutations (Asn to Gln) and found that six out of eight sites were actually glycosylated (G2 to G7); one in the stalk (G2) and five in the globular head domain (G3 to G7). We then tested the roles of individual and combined HeV G N-glycan mutants and found functions in the modulation of shielding against neutralizing antibodies, intracellular transport, G-F interactions, cell-cell fusion, and viral entry. Between the highly conserved HeV and NiV G glycoproteins, similar trends in the effects of N-glycans on protein functions were observed, with differences in the levels at which some N-glycan mutants affected such functions. While the N-glycan in the stalk domain (G2) had roles that were highly conserved between HeV and NiV G, individual N-glycans in the head affected the levels of several protein functions differently. Our findings are discussed in the context of their contributions to our understanding of HeV and NiV pathogenesis and immune responses.

IMPORTANCE

Viral envelope glycoproteins are important for viral pathogenicity and immune evasion. N-glycan shielding is one mechanism by which immune evasion can be achieved. In paramyxoviruses, viral attachment and membrane fusion are governed by the close interaction of the attachment proteins H/HN/G and the fusion protein F. In this study, we show that the attachment glycoprotein G of Hendra virus (HeV), a deadly paramyxovirus, is N-glycosylated at six sites (G2 to G7) and that most of these sites have important roles in viral entry, cell-cell fusion, G-F interactions, G oligomerization, and immune evasion. Overall, we found that the N-glycan in the stalk domain (G2) had roles that were very conserved between HeV G and the closely related Nipah virus G, whereas individual N-glycans in the head quantitatively modulated several protein functions differently between the two viruses.

Hendra virus (HeV), Nipah virus (NiV), and the newly discovered Cedar virus (CedPV) belong to the genus *Henipavirus* in the *Paramyxoviridae* family (1, 2). HeV and NiV are emerging zoonotic viruses that can be transmitted from bats to humans directly or via intermediary hosts. These are the only two viruses in the *Paramyxoviridae* family classified as biosafety level 4 (BSL4), and their mortality rates in humans are 40 to 75% (3). HeV is transmitted to horses via fruit bats, and several outbreaks in horses have been reported as recently as 2014 (4, 5). Although HeV outbreaks have been rare and limited to eastern Australia, the high mortality rates of henipaviruses in humans and the broadening of fruit bat habitats raise serious concerns about the spread of these viruses (6). Vaccines and postexposure treatments targeting the soluble form of HeV G (sG_{HeV}) seem promising, but to date, a vaccine has only been licensed for use in horses (EquivacHeV) (7, 8). More detailed structural and functional analyses of the Hendra virus G glycoprotein may help us improve vaccine approaches and our understanding of HeV and NiV pathobiology.

The paramyxoviruses have two surface glycoproteins, the attachment (H/HN/G) and fusion (F) glycoproteins. These proteins work in concert; thus, in the case of NiV or HeV, the binding of G to a cellular receptor (ephrin B2/ephrin B3) induces a recently described conformational cascade in G that ultimately triggers F to execute pH-independent virus-cell or cell-cell membrane fusion (9–11). The attachment protein is a type II transmembrane glycoprotein with a predicted N-terminal cytoplasmic tail (residues 1 to 46), a transmembrane domain (residues 47 to 69), and a C-terminal ectodomain (residues 70 to 604). The HeV G ectodomain is divided into the stalk region (residues 71 to 188) and the globular head domain (residues 189 to 604) (Fig. 1A) (12, 13).

NiV G is heavily glycosylated, with six of the seven potential N-linked glycosylation sites being utilized (G2 to G7) (14). G2 is located in the stalk region (residue 159), whereas the remaining N-glycosylation sites (G3 to G7) are located on the surface of the globular head domain (15). The NiV and HeV G proteins share 83% amino acid identity and utilize the same cell entry receptors,

Received 20 March 2015 **Accepted** 27 April 2015

Accepted manuscript posted online 6 May 2015

Citation Bradel-Tretheway BG, Liu Q, Stone JA, McInally S, Aguilar HC. 2015. Novel functions of Hendra virus G N-glycans and comparisons to Nipah virus. J Virol 89:7235–7247. doi:10.1128/JVI.00773-15.

Editor: D. S. Lyles

Address correspondence to Hector C. Aguilar, haguilar@vetmed.wsu.edu.

doi:10.1128/JVI.00773-15

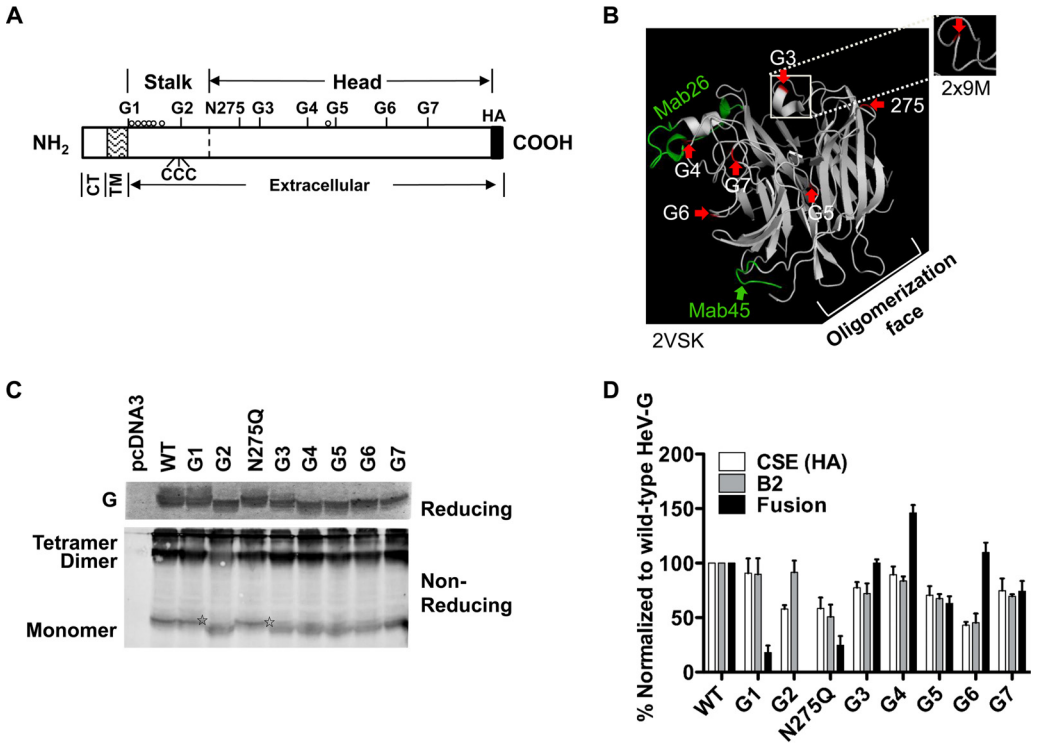

FIG 1 Individual characterizations of all eight predicted N-glycosylation sites in HeV G. (A) Schematic representation of HeV G, including the positions of the eight potential glycosylation sites. The cytoplasmic tail (CT), transmembrane (TM), and extracellular domains of HeV G are indicated. Three cysteine residues in the stalk domain that are important for G oligomerization are depicted (CCC) (13). O-glycosylation sites published for HeV G are illustrated by open circles (24). (B) N-glycan structural positions in the head of HeV G. Side view of the cartoon representation of the monomeric subunit structure of the HeV G globular head domain, taken from HeV G in complex with ephrin B2 (PDB ID 2VSK) (38). Interestingly, the G3 region from the dimeric crystal structure of HeV G (PDB ID 2X9M) (39) shows this region to form a loop (outer box) instead of an alpha helix (inner box). Structures were attained using PYMOL (www.pymol.org). The structure displays the positions of the predicted HeV G head N-glycosylation sites (G3 to G7 and position 275, highlighted in red and marked by red arrows). The likely oligomerization face of HeV G (39) is indicated. The MAb26 and MAb45 binding regions (11) are highlighted in green. (C) 293T cells were transfected with WT or mutant HeV G expression constructs and lysed 20 to 24 h posttransfection. Lysates were analyzed for HeV G expression by reducing (top gel) or nonreducing (bottom gel) PAGE and subsequent immunoblotting against the C-terminal HA tag in HeV G using rabbit anti-HA antibody. The reducing gel resolved the monomeric form of HeV G, whereas the nonreducing gel also resolved the dimeric and tetrameric forms of HeV G, as indicated. Stars denote the monomeric G of the unoccupied N-glycosylation sites of the G1 and N275Q mutants, running with the same mobility as WT HeV G. (D) 293T cell surface expression (CSE) and ephrin B2 (B2) receptor binding of HeV G N-glycan mutants was determined by flow cytometry using mouse anti-HA antibody or soluble mouse ephrin B2/Fc chimeric protein, respectively. The fusion promotion abilities of the HeV G N-glycan mutants were assessed in 293T cells by cotransfection with WT HeV F. Syncytial nuclei were counted as outlined in Materials and Methods. The CSE, ephrin B2 binding, and fusion levels of the HeV G N-glycan mutants were normalized to those of WT HeV G. Data shown are the average results ± standard errors of the means (SEM) from at least three independent experiments.

ephrin B2 and ephrin B3, although HeV G binding seems to have lower avidities, particularly with ephrin B3 (16–18). The predicted N-glycosylation sites are mostly conserved between NiV and HeV G, except that HeV G harbors an additional predicted glycosylation site at residue 275. However, the residues actually N-glycosylated in HeV G and the potential biological roles of the actual HeV G N-glycans are currently not known.

In this study, we conservatively mutated the eight potential HeV G N-glycosylation sites and identified those actually N-glycosylated. In addition, we discovered several HeV G N-glycan modulatory functions in viral entry, cell-cell fusion, interactions with F, and shielding from neutralizing antibodies. These important roles in HeV biology highlight many similarities and some quantitative differences compared to the NiV G N-glycan functions.

MATERIALS AND METHODS

Expression plasmids and site-directed mutagenesis. Codon-optimized F and G pcDNA3.1 expression plasmids for NiV and HeV were constructed as previously described (19). Upon inspection of the GenBank database, we found that two main published HeV G amino acid sequences exist, differing by single amino acid residues at position 134 in the stalk and position 507 in the globular head domain (GenBank accession numbers AAV80426.1 and AEQ38115.1). To reflect the most common sequence in the database, the Hendra virus G expression construct (AAV80426.1) was modified at residues 134 (C to S) and 507 (S to T) using site-directed mutagenesis. Note also that the threonine at residue 507 of HeV G increases ephrin B3 binding levels close to those of NiV G (16).

Conserved asparagine-to-glutamine mutations were introduced at each predicted glycosylation site by standard site-directed mutagenesis at amino acid positions 72 (G1), 159 (G2), 275 (N275Q), 306 (G3), 378 (G4), 417 (G5), 481 (G6), and 529 (G7) in the HeV G glycoprotein. The sequences were verified by DNA sequencing (Eurofins, AL). HeV G genes were cloned within the NotI and KpnI restriction sites of the pcDNA3.1(-) vector (Invitrogen, NY), and the HeV F gene was cloned within KpnI and XhoI restriction sites of the pCAGGS vector.

Cell lines. PK13 and 293T cells were maintained in Dulbecco's modified Eagle's medium (DMEM), and Vero cells were cultured in minimal essential medium (MEM), both supplemented with 10% fetal bovine se-

rum (FBS), 50 IU penicillin ml^{-1}, 50 μg streptomycin ml^{-1}, and 2 mM glutamine.

Cell-cell fusion assay. HEK293T cells (~70% confluence) were transfected with wild-type (WT) HeV F and WT or mutant HeV G expression plasmids (1:1 ratio). Syncytial nuclei (4 or more nuclei per cell) were counted in each microscopic field (200×). Five microscopic fields were counted for each transfection (11, 20).

Quantification of HeV G cell surface expression, ephrin B2, and conformational antibody binding by flow cytometry. 293T or ephrin B2-deficient PK13 cells were transfected with 2 μg WT or mutant HeV G expression plasmids and collected at 20 to 24 h posttransfection. Cells transfected with vector alone (pcDNA3.1) served as a negative control. To measure cell surface expression and ephrin B2 binding levels, 293T cells expressing WT or mutant HeV G proteins were incubated with mouse antihemagglutinin (anti-HA) antibody (1:400; Covance, PA) or a soluble recombinant mouse ephrin B2/human Fc chimera (10 nM; R&D Systems, MN) at 4°C for 1 h, respectively. Cells were washed twice with fluorescence-activated cell sorting (FACS) buffer (1% FBS in phosphate-buffered saline [PBS]) and incubated with Alexa Fluor 647-labeled anti-human or anti-mouse antibodies (1:400; Life Technologies, NY) for 30 min at 4°C. Cells were washed twice as before, fixed in 0.5% paraformaldehyde, and analyzed by flow cytometry (Guava easyCyte8 HT; EMD Millipore, MA). The soluble mouse ephrin B2/human Fc chimera contains the ectodomain of mouse ephrin B2 (residues 27 to 227).

For the conformational antibody binding assay, we used rabbit anti-NiV G monoclonal antibodies (MAb) MAb26 and MAb45, detecting both NiV G and HeV G (21). PK13 cells were transfected as described above. Cells were first incubated for 15 min at 4°C with 0 nM or 100 nM soluble ephrin B2 and then incubated for 1 h at 37°C with MAb26 or MAb45 (1:1,000 dilution). Bound antibody was detected using Alexa Fluor 647-labeled goat anti-rabbit antibody (Life Technologies, NY) at a dilution of 1:200. Cells were washed with FACS buffer and fixed as described above before analysis by flow cytometry (20, 22).

Reducing/nonreducing SDS-PAGE and immunoblotting. 293T cells were transfected with WT HeV F and/or WT or mutant HeV G expression plasmids and lysed in 1× radioimmunoprecipitation assay (RIPA) buffer (EMD Millipore, MA) supplemented with protease inhibitors (cOmplete mini; Roche, IN) 20 to 24 h posttransfection. Cell lysates or vesicular stomatitis virus (VSV)/HeV-rLuc (containing the *Renilla* luciferase reporter gene) pseudotyped virions were subjected to SDS-PAGE and immunoblotting. Amounts of 2×10^9 or 5×10^9 virions (genome copies) were separated by reducing (10%) or nonreducing (8%) SDS-PAGE, respectively. For nonreducing SDS-PAGE, samples were neither treated with β-mercaptoethanol nor denatured by heat. HeV G and F proteins were detected using anti-HA (1:2,000) or anti-AU1 (1:500) antibody (detecting the epitope tag DTYRYI), respectively. Fluorescently labeled secondary antibodies (1:2,000) were used as described above, and proteins were detected and quantitated using a ChemiDoc MP imaging system with ImageLab software (Bio-Rad, CA).

Coimmunoprecipitations. Equal amounts of F and G expression plasmids (6 μg each) were transfected into HEK293T cells (~90% confluence in 10-cm dishes) using BioT (Bioland Scientific, CA). The expression of only F or G was used as the respective negative control. Approximately 20 h posttransfection, cells were washed with PBS and lysed in 1.5 ml RIPA buffer (Millipore, MA) supplemented with complete protease inhibitor (cOmplete mini; Roche, IN). Cells were lysed for 20 min on ice, and cellular debris was precleared by centrifugation. One half of the cell lysate was utilized for immunoprecipitation using the μMACS HA isolation kit (Miltenyi Biotec, CA). Briefly, lysates were incubated with 35 μl of μMACS protein G MicroBeads by rotating at 4°C for 1 h. HA-tagged proteins were bound to μMACS columns, washed at least four times with RIPA buffer supplemented as described above, and eluted in hot SDS-loading dye (Laemmli buffer) containing 0.1 M mercaptoethanol as recommended by the manufacturer. Half of each purified elution was separated by 10% PAGE and blotted onto a polyvinylidene difluoride (PVDF) membrane. F and G proteins were detected using anti-mouse AU1 antibody (1:500) and anti-rabbit HA antibody (1:2,000), respectively, and fluorescent secondary antibodies (Alexa Fluor 488-labeled goat anti-mouse and Alexa Fluor 647-labeled goat anti-rabbit antibodies, respectively; Life Technologies, NY) were used as described above (1:4,000). Actin was used as an internal loading control for lysate samples using rabbit antiactin (I-19; Santa Cruz, CA) polyclonal antiserum at a 1:200 dilution. Western blots were imaged with the ChemiDoc XRS system (Bio-Rad, CA), and protein bands were quantified using ImageLab analysis software (Bio-Rad, CA).

Pseudotyped HeV/VSV-rLuc production, qPCR, and viral entry assay. Virus stocks were produced in HEK293T cells essentially as described previously (17, 20). Briefly, 293T cells were transfected with WT HeV F and WT or mutant HeV G expression plasmids at a 1:1 ratio and the following day infected with recombinant VSV-ΔG-rLuc (VSV that lacks its own glycoprotein but contains the *Renilla* luciferase reporter gene). HeV/VSV-rLuc pseudotyped virions were collected at roughly 24 h postinfection and purified over a 20% sucrose cushion. Virions were resuspended in NTE buffer (150 mM NaCl, 40 mM Tris-HCl, 1 mM EDTA, pH 8.0) supplemented with 5% sucrose and stored at −80°C. Viral RNA was extracted using the QIAamp viral RNA minikit (Qiagen, CA), and the isolated RNA was reverse transcribed using the SuperScript III first-strand synthesis system for RT-PCR (Invitrogen, NY). The VSV genome copy numbers were quantified by using a quantitative PCR (qPCR) TaqMan protocol as previously described (20).

To quantify viral entry, Vero cells were seeded in a 96-well plate and infected at 30 to 50% confluence using 10-fold serial virus dilutions. Infections were done for 2 h in infection medium (PBS plus 1% FBS). Complete growth medium (MEM) was then added to the cells, which were lysed 20 to 24 h postinfection. Luciferase activity was then measured as relative light units (RLU) using a *Renilla* luciferase flash assay kit (Pierce) and an Infinite M1000 microplate reader (Tecan Group Ltd., Männedorf, Switzerland). RLU were plotted against genome copies per ml and regressed using GraphPad Prism 5 (GraphPad Software, Inc., CA).

Antibody neutralization assays and statistical analysis. Pseudotyped HeV/VSV-rLuc virions carrying WT or mutant HeV G and WT HeV F were normalized to equivalent viral genome copy numbers (10^8 copies) as determined by quantitative real-time PCR. Viruses were then incubated for 20 min in infection medium (1% FBS in PBS) in the presence of various dilutions (ranging from 10^{-2} to 10^{-6}) of HeV G rabbit polyclonal antiserum 837. Antiserum 837 was produced against virus-like particles (VLPs) containing NiV M and HeV F and codon-optimized HeV G in New Zealand White rabbits, similar to a previously described method for the production of NiV-specific antisera (17). The antibody/virus mixture was added to Vero cells (30 to 50% confluence) and incubated for 2 h. The cells were then incubated in complete growth medium overnight and lysed 20 to 24 h postinfection. The luciferase expression was then measured as described in the section above. To calculate statistical differences in antibody neutralization among different N-glycan HeV G mutants, we used data obtained with the antiserum dilution of 10^{-4}, since this dilution had close to 50% inhibitory concentration (IC_{50}) for most pseudotyped viruses. An unpaired two-tailed Student's *t* test was applied by comparing the results for the WT to those for each N-glycan mutant virus.

RESULTS

The HeV G attachment protein is glycosylated at six of its eight potential N-glycosylation sites. The Hendra virus attachment glycoprotein (HeV G) is a type II transmembrane protein with an N-terminal intracellular domain, a transmembrane domain, and an extracellular domain that encompasses a stalk region and a C-terminal globular head (Fig. 1A). HeV G shares seven predicted N-glycosylation sites (NXS/T) with NiV G (G1 to G7), located at Asn residues 72, 159, 306, 378, 417, 481, and 529, in addition to N275, not present in NiV G (Fig. 1A) (14). Most of the G N-glycosylation sites are located in the head domain, with the exception

of G1 and G2, which are located in the stalk domain (Fig. 1A). The N-glycosylation sites in the HeV G head are generally located on surface-exposed loops, as shown in an HeV G head crystal structure cartoon model (Fig. 1B).

To identify the potential N-glycosylation sites that are actually N-glycosylated in HeV G, we mutated each of the eight predicted glycosylation sites (G1 to G7 and N275) via a conservative mutation of Asn (N) to Gln (Q). We previously confirmed for NiV G that a single N-to-Q substitution in an actual glycosylation site results in a loss of N-glycosylation and a mobility shift of 2 to 3 kDa, visible upon SDS-PAGE analysis (14). Hence, we transfected wild-type (WT) or mutant HeV G constructs into 293T cells and tested for protein expression 20 to 24 h posttransfection. Cells were lysed, and proteins were separated by reducing or nonreducing SDS-PAGE and detected by immunoblotting that targeted the C-terminal HA epitope tag in HeV G. All constructs were expressed at levels roughly similar to the level of G (Fig. 1C, top gel), and an expected mobility shift of 2 to 3 kDa could be seen for the monomeric form of all mutants except G1 and N275Q (Fig. 1C). Thus, the N-glycosylation sites that were actually N-glycosylated (G2 to G7) were found to be identical in HeV G and NiV G (14). All mutants were able to form monomeric, dimeric, and tetrameric forms of G when separated under nonreducing conditions (Fig. 1C, bottom gel), although the dimeric form was represented at reduced levels for G2 (19 to 20% of total G) compared to its level for WT G (32 to 56% of total G).

Removal of N-glycans in the head of HeV G enhances cell-cell fusion promotion, whereas removal of the N-glycan in the stalk decreases it. Cell membrane fusion induced by HeV is a process that involves cell surface-expressed G protein binding to cellular receptors ephrin B2 and ephrin B3. Receptor engagement leads to successive conformational changes in G and F, which ultimately result in cell-cell fusion. Therefore, we next tested whether N-glycosylation is important for cell-cell fusion by cotransfecting the WT or mutant HeV G expression constructs with WT HeV F into 293T cells. As previously established, we then counted the number of syncytial nuclei per field (200× magnification, five fields for each mutant, $n > 3$) and normalized this number to the number for WT HeV fusion, which was set at 100% (Fig. 1D) (11, 20). We observed apparent effects of several N-glycan mutants on the levels of cell-cell fusion induced compared to the level induced by WT HeV G.

Since fusion is dependent on cell surface expression of G, we next asked whether all HeV G mutants were efficiently transported to the cell surface (23). Notably, we previously showed that when transfecting with the amounts of DNA used in this study, there is a linear relationship between cell surface expression and syncytium formation (20). The cell surface expression (CSE) levels of the HeV G mutants were also analyzed in 293T cells by flow cytometry, detecting the C-terminal HA epitope tag in HeV G (Fig. 1D). N-glycan mutant CSE levels were normalized to the level for WT HeV G, which was set to 100%. The mutant CSE levels varied from 45% (G6) to WT levels (G1 and G4) (Fig. 1D). This indicates that some N-glycans are more important than others for proper folding into a transport-competent conformation.

To account for differences in CSE levels influencing the levels of cell-cell fusion, we also determined each mutant's fusion index (FI), by calculating the ratio of normalized fusion levels to normalized CSE levels (fusion/CSE ratios) (all levels are summarized in Table 1). Compared to WT HeV G (FI of 1), the G4, G6, and to a lesser extent, G3 mutants were hyperfusogenic (FIs of 1.64, 2.55, and 1.29, respectively), whereas the stalk G2 mutant was fusion dead (FI of 0.00). Interestingly, the other stalk mutant, the G1 mutant, also displayed a hypofusogenic phenotype (FI of 0.20) even though this site appeared to be nonglycosylated (Fig. 1A and C). These results indicate that N-to-Q changes in the stalk region (residues 72 [G1] and 159 [G2]), including the removal of a stalk N-glycan (G2), have a profound impact on the fusion abilities of HeV G, whereas the removal of N-glycan G3, G4, or G6 in the head leads to higher fusion levels than for WT HeV G.

We then analyzed whether the removal of specific N-glycans affects the binding of HeV G to its cellular receptor ephrin B2, as previous literature indicated that, for example, the N-glycan at position 529 (G7) is near the ephrin B2 binding site in HeV G, potentially affecting receptor attachment (24). Ephrin B2 binds to the upper face of the HeV G head, and the exact binding pockets in HeV G have been previously described (25). We found that all HeV G N-glycan mutants were able to bind soluble ephrin B2 at levels roughly corresponding to their CSE levels, with the exception of the G2 stalk mutant, which showed a 1.6-fold increase in binding to ephrin B2 compared to its CSE level (Fig. 1D). This indicates that the efficiency of ephrin B2 binding is not dependent on N-glycosylation at most N-glycosylation sites in HeV G. Importantly, this also shows that the N-glycan mutants' effects on cell-cell fusion were not due to aberrant levels of ephrin B2 binding.

TABLE 1 Fusion indices for HeV G wild-type and N-glycan mutant glycoproteins and comparison to published NiV G fusion indices[a]

G env	HeV G			NiV G (FI ± SEM)[b]
	CSE	Fusion	FI ± SEM	
WT	100	100	1.00	1.00
N-glycan mutants				
G1	90	18	0.20 ± 0.07	0.31 ± 0.06
G2	58	0	0.00 ± 0.00	0.02 ± 0.03
N275Q	58	25	0.43 ± 0.14	ND
G3**	77	100	**1.29 ± 0.04**	**0.86 ± 0.11**
G4**	89	146	**1.64 ± 0.08**	**1.11 ± 0.10**
G5	70	63	0.89 ± 0.09	0.67 ± 0.06
G6**	43	110	**2.55 ± 0.21**	**6.38 ± 0.45**
G7**	75	74	**0.99 ± 0.13**	**1.60 ± 0.09**
G2G3	31	0	0.00 ± 0.00	0.10 ± 0.06
G3G4	57	120	2.11 ± 0.25	ND
G3G5	39	98	2.47 ± 0.47	ND
G4G5	37	102	2.91 ± 0.26	2.50 ± 0.29
G6G7**	12	33	**2.38 ± 0.13**	**1.46 ± 0.09**
G4G7*	28	84	**3.02 ± 0.35**	**4.13 ± 0.21**
G3G4G5**	15	173	**11.81 ± 1.09**	**4.49 ± 0.54**
G4G5G6	2	0	—	5.88 ± 0.41
G4G6G7	1	1	—	6.71 ± 0.43
G3G4G5G6	0	0	—	ND

[a] Statistical analysis was done using the Student *t* test (two-sample assuming equal variances). Statistically significant differences between FIs (fusion indices [fusion/CSE ratios]) from both viruses are indicated by boldface and by asterisks as follows: **, $P < 0.01$; *, $P < 0.05$. —, sample for which a valid FI could not be determined due to no or minimal surface expression; ND, not determined; CSE, cell surface expression; WT, wild type G.

[b] NiV G FIs were previously published by Biering et al. (14), with the exception of NiV G3G4G5, which was determined in this study.

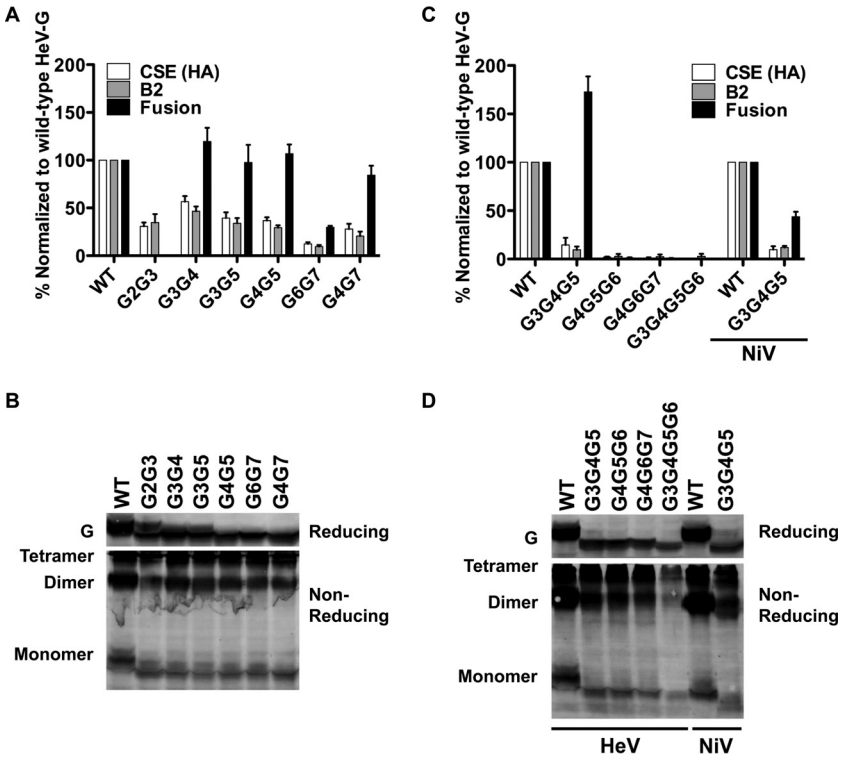

FIG 2 The removal of two or more N-glycans in HeV G leads to hypo- and hyperfusogenic phenotypes. (A, C) 293T cell surface expression (CSE) and ephrin B2 (B2) receptor binding of HeV G N-glycan double (A) and multiple mutants (C) were determined by flow cytometry using mouse anti-HA antibody (CSE) and soluble mouse ephrin B2/Fc chimera, respectively. Experiments were done similarly to those described in the legend to Fig. 1D. (B, D) N-glycan mutants were transfected into 293T cells and analyzed by reducing and nonreducing SDS-PAGE and subsequent Western blot analysis, similar to the experiments described in the legend to Fig. 1C. (C, D) Wild-type NiV G and the NiV G3G4G5 mutant were analyzed next to HeV G mutants. The results of one representative experiment out of three independent experiments are shown for each.

Simultaneous removal of multiple N-glycosylation sites in HeV G severely affects protein expression, CSE, and membrane fusion. To determine whether the effects of N-glycans on CSE and/or fusion promotion abilities may be cumulative, synergistic, antagonistic, dominant, and/or recessive, we next mutated two or more N-glycosylation sites simultaneously (Fig. 2A and C). We chose the N-glycan multiple mutants according to the hyper- or hypofusogenic phenotypes of the HeV G N-glycan single mutants and some N-glycan mutations previously published for NiV G (Table 1) (14). The CSE levels of the double mutants ranged from 12% (G6G7) to 57% (G3G4) and were all substantially lower than the CSE levels of their individual mutant counterparts (Fig. 2A; Table 1). Similarly, abolishing three or more N-glycan sites in HeV G further reduced CSE levels, now ranging from 0% (G3G4G5G6 mutant) to 15% (G3G4G5 mutant) (Fig. 2C; Table 1). Again, the ephrin B2 binding levels were comparable to the CSE levels for each mutant, indicating that ephrin B2 binding was not noticeably affected by N-glycan removal.

Next, we determined the fusogenic properties of the double, triple, and quadruple N-glycan mutants (Fig. 2A and C). The hypofusogenic phenotype seen for mutant G2 likely is a dominant phenotype, since again a fusion-dead phenotype was observed when the G2 mutation was combined with the hyperfusogenic G3 mutation (the G2G3 mutant's FI was 0.00). Furthermore, we examined the N-glycan mutant combinations in the HeV G head and observed that all combinations analyzed yielded enhanced hyperfusogenic phenotypes (FIs ranging from 2.11 to 3.02) compared to the phenotype of WT HeV G (Fig. 2A). The effect was even more pronounced for the G3G4G5 triple mutant, which yielded a strongly hyperfusogenic phenotype, with a fusion index of 11.81. However, our data also indicated that there is a limit to how many N-glycans in HeV G can be removed, as all the other triple and quadruple N-glycan mutants yielded nearly fusion-dead phenotypes in 293T cells, likely due to their overall extremely low CSE levels (ranging from 0 to 2%) (Fig. 2C; Table 1).

All of the double, triple, and quadruple N-glycan mutants analyzed had different degrees of reduction of total cell expression and CSE levels compared to those of WT HeV G, as detected by Western blot analysis (Fig. 2B and D) and flow cytometry (Fig. 2A and C), respectively. In general, the reduction in protein expression was directly proportional to the number of N-glycans removed, with the least amount of protein expression for the G3G4G5G6 quadruple mutant. Most importantly, the removal of multiple N-glycans generally resulted in increased levels of cell-cell fusion, provided that a minimum level of CSE of more than approximately 10% was reached for a given mutant.

Furthermore, all HeV G multiple N-glycan mutants were able to form monomeric, dimeric, and tetrameric species similarly to WT HeV G, suggesting that the mutations did not significantly affect the oligomeric folding ability of the G mutants (Fig. 2B and D, bottom gels). The exception was the G2G3 mutant, which, similarly to the G2 mutant (Fig. 1C), yielded a lower proportion of dimers (17 to 20%) than the WT G (32 to 56%). Since the G3G4G5 triple mutant yielded the highest fusion index (11.81),

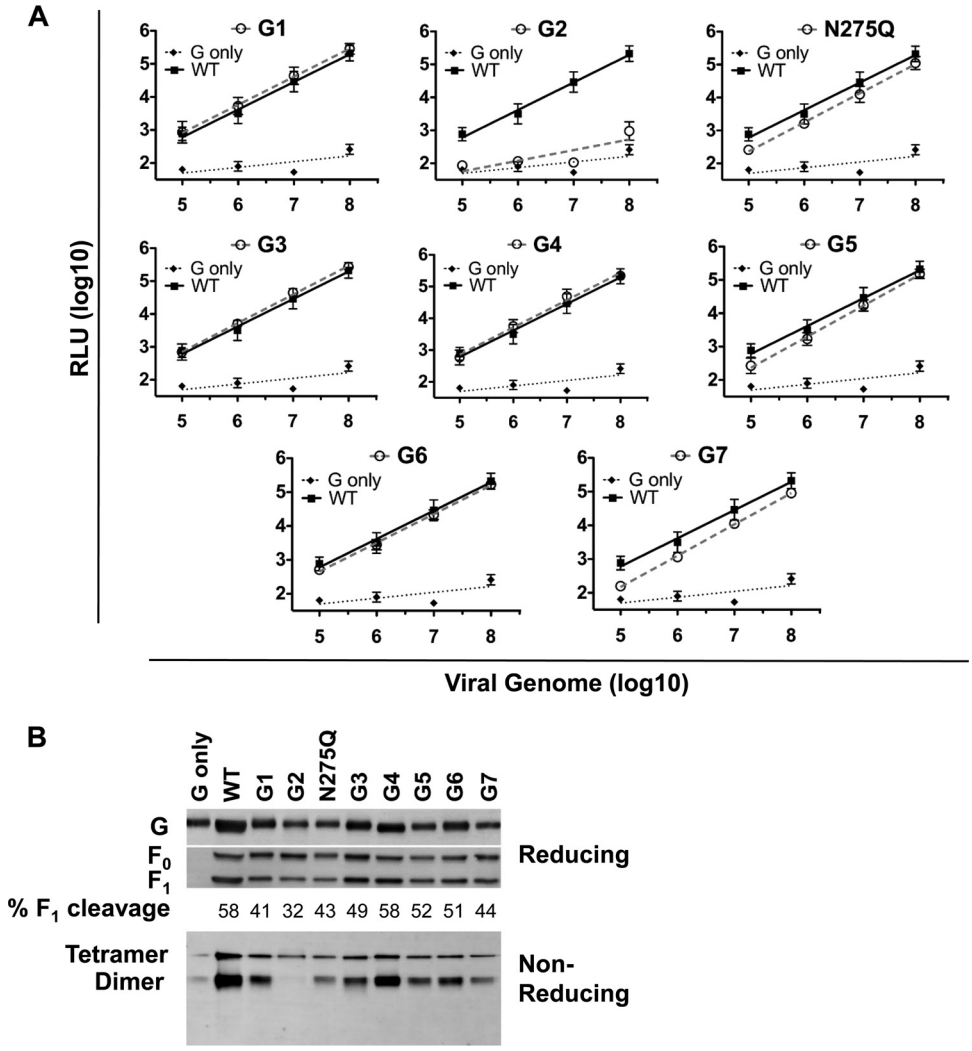

FIG 3 The removal of individual N-glycans in HeV G modulates viral entry and oligomerization of G. (A) Viral entry assay. Vero cells were infected with serial dilutions of HeV/VSV-rLuc pseudotyped virions containing either WT or mutant HeV G in combination with or without HeV F (G only). Cells were lysed 20 to 24 h postinfection, and relative light units (RLU) were quantified and plotted against the number of viral genomes/ml. Virions produced with HeV F only or empty vector yielded viral entry levels similar to those of G-only virions (data not shown). Data shown are the average results ± SEM from at least three independent experiments. (B) Mutant HeV G virus incorporation and oligomerization. HeV/VSV-rLuc pseudotyped virions as used in the experiment whose results are shown in panel A were separated by reducing or nonreducing SDS-PAGE and immunoblotted against G (rabbit anti-HA antibody)- and F (mouse anti-AU1 antibody)-specific antibodies. Oligomeric forms of G are indicated. Note that no monomeric form was separated by nonreducing SDS-PAGE when samples were obtained from virions. The percentages of F_1 cleavage were determined by densitometry. The results of one representative experiment out of three independent experiments are shown.

we were interested in a comparison with a homologous NiV G mutant. The NiV G triple mutant also resulted in a hyperfusogenic phenotype; however, its fusogenic capabilities were lower than those of its HeV counterpart (FI of 4.49). The differences and similarities between fusion indices obtained for HeV G N-glycan mutants and previously published indices for NiV G N-glycan mutants are summarized in Table 1.

HeV G N-glycans modulate viral entry, incorporation of F into virions, and assembly of G into higher oligomeric structures. It is thought that the mechanism for viral entry (viral-cell membrane fusion) is generally closely related to the mechanism for cell-cell fusion (cell-cell membrane fusion) (26). We were interested in determining whether HeV G N-glycan mutants would have similar cell-cell fusion and viral entry phenotypes. Thus, we analyzed single and multiple N-glycan mutants of HeV G for their ability to induce viral entry into Vero cells (Fig. 3A and 4A, respectively). To do so, we made use of our previously established BSL2 pseudotyped viral entry assay. Briefly, WT or mutant HeV G proteins were pseudotyped together with WT HeV F onto vesicular stomatitis virus (VSV) that lacks its own glycoprotein but contains the *Renilla* luciferase reporter gene (VSV-ΔG-rLuc) (20, 22). Pseudotyped virus carrying WT HeV G but lacking WT HeV F (denoted in figures as "G only") was used as a negative-control virus to control for nonspecific entry of virions via nonviral/cell membrane fusion mechanisms. We constructed HeV/VSV-rLuc virions for all of the single and double mutants for which schematics and experimental results are shown in Fig. 1 and 2A, respectively, along with the hyperfusogenic G3G4G5 triple mutant (Fig. 2C). To accurately compare viral entry levels, we determined pseudotyped VSV genome concentrations by using quantitative

reverse transcription-PCR (see Materials and Methods), as previously established (20). We normalized the amounts of WT and mutant HeV/VSV-rLuc virions to the equivalent viral genome copy numbers and used 10-fold serial dilutions to infect Vero cells. Cells were lysed 20 to 24 h postinfection and monitored for luciferase activity, a direct measurement of viral entry.

Generally, the cell-cell fusion levels correlated with the levels of viral entry (Fig. 3A and 4A). The hypofusogenic G2 stalk mutants (G2 and G2G3 mutants), for example, had viral entry levels close to that of the negative-control virus (G only) (Fig. 3A and 4A, respectively). All the HeV G head mutants had close to WT HeV G viral entry levels, with the exception of all G7 mutants (G7, G6G7, and G4G7 mutants), which had somewhat lower levels of viral entry (0.5 to 1 log) than WT HeV G virions, even though their cell-cell fusion levels were equal to or greater than the WT fusion levels. We then postulated that the reduced viral entry levels for these virions were likely due to reduced levels of incorporation of the mutant G onto the virions. PAGE and immunoblotting with anti-F (anti-AU1)- or anti-G (anti-HA)-specific antibodies showed that the levels of G incorporation into virions were indeed lower for the G7, G6G7, and G4G7 mutants than for WT HeV G (Fig. 3B and 4B, top). Notably, the G1 stalk mutant pseudotyped virions were able to enter cells at WT levels despite a hypofusogenic cell-cell fusion phenotype of the G1 mutant (Fig. 1C and 3A; Table 1). Also, we noticed somewhat lower levels of incorporation of the G1 mutant into virions than for the WT (Fig. 3B). Similar results were previously observed for the NiV G1 mutant, which indicates that viral entry and cell-cell fusion mechanisms may not necessarily be as equivalent as previously thought (14).

Next, we asked whether G N-glycan mutants that were incorporated into pseudotyped virions were of higher oligomeric structures, like those observed in the cell lysates (Fig. 1C and 2B and D). We separated virions by nonreducing PAGE and performed immunoblotting with anti-G (anti-HA)-specific antibodies (Fig. 3B and 4B and C). All mutants except the G2 mutant were able to form dimeric and tetrameric G similarly to WT HeV G. In contrast, the HeV/VSV-rLuc virions containing the G2 mutations (G2 and G2G3 mutants) had significantly reduced proportions of dimeric G (8 to 26%) compared to its proportion for the WT (66 to 75%) or any of the other mutant G virions (59 to 75%) (Fig. 3B and 4B, respectively). These results suggest that the G2 N-glycan in the HeV G stalk (residue 159) is crucial for proper folding of HeV G and that removal of the G2 N-glycan results in a reduction of dimeric G, presumably due to increased tetrameric stability. In addition, viral incorporation of monomers was basically undetectable for WT or mutant G proteins, suggesting that higher oligomers are selectively incorporated into virions (Fig. 3B and 4B).

Additionally, since the most hyperfusogenic HeV G N-glycan mutant was the G3G4G5 triple mutant, we were interested in comparing it to its NiV G counterpart, since it had not been previously analyzed. Thus, we prepared WT or mutant NiV G/VSV-rLuc virions containing WT-NiV F in combination with either WT NiV G or the NiV G3G4G5 mutant protein, as well as a negative-control virus that contained WT NiV G only. Overall, WT NiV G pseudotyped virions (NiV WT) appeared to have slightly enhanced entry levels compared to those of HeV G (WT) pseudotyped virions (Fig. 4A), which might be due to increased incorporation of NiV G into pseudotyped NiV WT virions (Fig. 4C). The NiV G3G4G5 pseudotyped virions entered at approximately NiV G WT levels (Fig. 4A). The virion entry levels were enhanced for HeV and NiV G3G4G5 mutant virions compared to the entry levels of their wild-type G counterparts, which is notable considering the reduced viral incorporation levels of F and G glycoproteins onto these mutant virions (Fig. 4C). Additionally, it is interesting that the G3G4G5 mutation in either HeV G or NiV G also affected the level of incorporation of WT F into virions, as measured by immunoblot analysis (Fig. 4C), indicating that certain N-glycans in the attachment protein G modulate the efficient incorporation of F into virus particles, presumably by affecting the G-F interactions.

HeV G N-glycans affect HeV G-F interactions. To analyze whether HeV G N-glycans affect the HeV G-F interactions, we performed coimmunoprecipitation studies from lysates of 293T cells cotransfected with G and F. Affinity purification was directed against the HeV G HA tag; therefore, only F that directly associated with G was coimmunoprecipitated by this method. We used μMACS anti-HA antibody-coated magnetic beads to specifically bind HA-tagged G proteins. Viral G and F proteins were detected from total cell lysates or from the immunoprecipitated (IP) fractions by immunoblotting using rabbit anti-HA and mouse anti-AU1 antibodies, respectively. Actin was detected as an internal loading control for the total cell lysate samples, whereas IgG (light chain) served as a loading control for the immunoprecipitated fractions (Fig. 5A). Interestingly, when analyzing F and G expression levels from total cell lysates, we found that the G2 and G2G3 stalk mutants lowered the total levels of expression of cotransfected WT HeV F by about 2.5-fold compared to the results for WT HeV G, as measured by densitometry (Fig. 5A, left). Next, we measured the total concentration of F (inactive precursor F_0 and activated proteolytic cleavage product F_1) in the cell lysate and in the eluate (IP fraction) by densitometry (Fig. 5A). Although due to the nature of these assays, these avidity measurements are only semiquantitative, we normalized the value for each mutant to the value for WT HeV G, set as 1. Then, we measured the avidities of the G-F interactions for the WT and mutant G proteins by calculating the ratio of coimmunoprecipitated HeV F to HeV F in total cell lysates (F IP fraction/F lysate) (20). The results shown in Fig. 5B and C are from at least four independent experiments.

We found that the strongly hypofusogenic G2 and G2G3 stalk mutants pulled down F at increased levels compared to the results for WT HeV G (the avidities of the G-F interactions were 8.9 and 10.3, respectively; $P < 0.05$) (Fig. 5B and C). Interestingly, these results suggest that there is an inverse correlation between fusogenicity and G-F interaction for HeV G N-glycan mutants, similar to that previously observed for NiV F N-glycan mutants (20).

HeV G stalk N-glycan mutants modulate receptor-induced conformational changes differently than WT HeV G. We previously described three receptor-induced conformational changes in NiV G that modulate cell-cell membrane fusion (11). These three conformational steps can be detected by using three different antibodies, MAb213 or MAb26 (step 1) and MAb45 (step 2) that bind to the head region of G and Ab167 (step 3) that binds to the stalk region of G (11, 21). Note that MAb213 and MAb26 have proximal epitopes in the head of G (within the region from residue 371 to 392), surrounding the G4 N-glycan region (Fig. 1B), but MAb213 and MAb26 both detect NiV G, whereas HeV G can only be detected by MAb26 (21). Here, we examined conformational steps 1 and 2, as steps 2 and 3 are spatiotemporally closely linked conformational changes (11, 27).

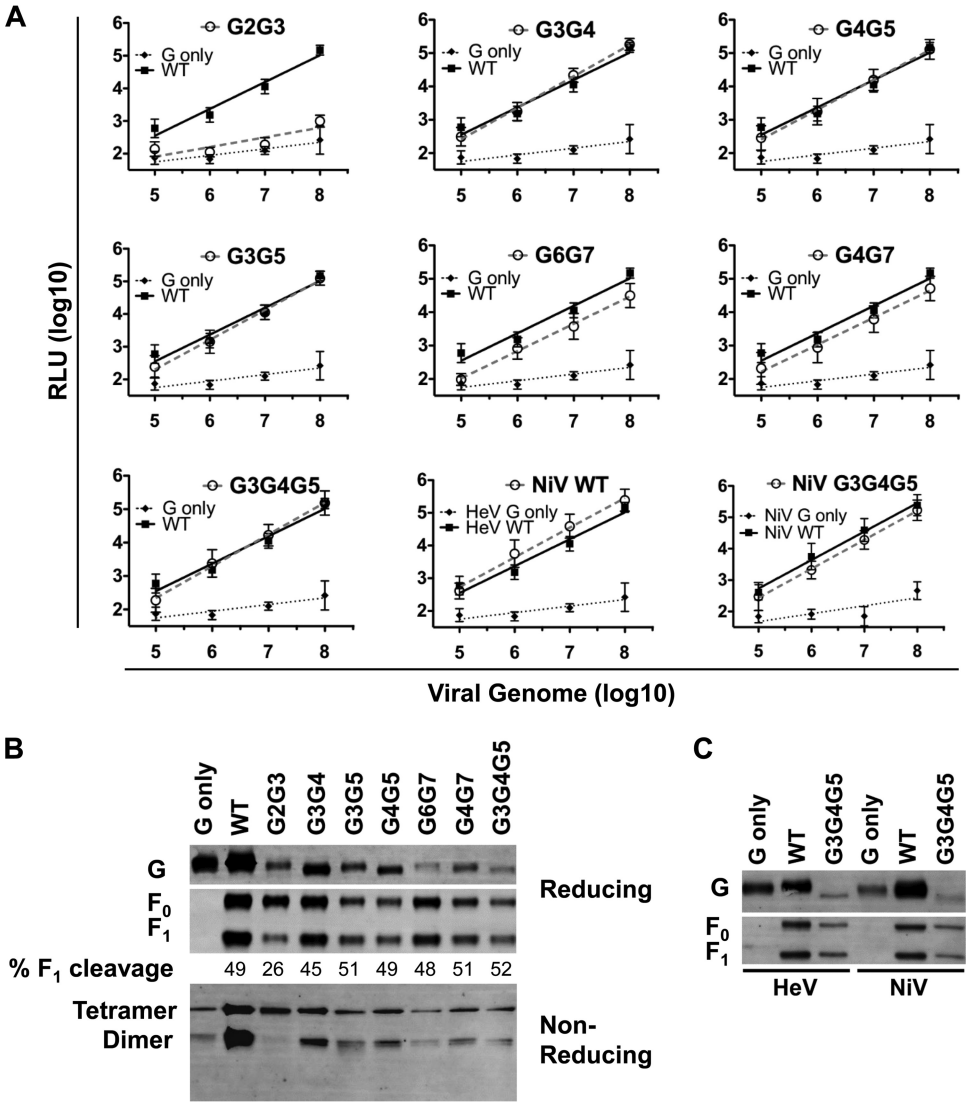

FIG 4 The removal of multiple N-glycans in HeV G modulates viral entry, oligomerization, and glycoprotein incorporation into the virus. (A, B) Viral entry (A) and viral incorporation and oligomerization levels (B) of HeV G mutants were detected in experiments similar to those described in the legend to Fig. 3A and B. (C) Comparison of levels of incorporation of WT and mutant HeV and NiV G into virions and their effects on homologous F incorporation. The data shown in panel A are the average results ± SEM from at least three independent experiments. The results of one representative experiment out of three are shown in panels B and C. The percentages of F_1 cleavage were determined by densitometry.

We first tested the binding of conformational antibodies to N-glycan mutants in their pre-receptor binding conformation. Thus, we detected the overall levels of MAb26 and MAb45 binding in the receptor-deficient cell line PK13, expressing single mutants and a subset of double mutants (Fig. 6A). We then calculated the relative antibody binding levels by comparing them to the corresponding cell surface expression (CSE) levels for each mutant (Fig. 6B). For the single mutants, we detected levels of binding to MAb26 and MAb45 that were roughly equal to their levels of CSE, except for the G2 mutant, which displayed enhanced binding for both MAb26 and MAb45 (~83% and 37% enhancement, respectively), and the G2G3 double mutant, which displayed enhanced MAb26 binding (29%). This is different from the other double mutants, which showed reduced binding to MAb26 (28 to 42%) or MAb45 (15 to 50%) compared to the results for WT HeV G.

After determining the conformational antibody binding to the pre-receptor protein conformation, we examined receptor-induced conformational changes in the HeV G N-glycan mutants. We detected the first conformational change (step 1) using MAb26. Previously, we showed that MAb213 or MAb26 binding to NiV G was reduced by ~70% upon ephrin B2 receptor engagement and that the reduction was not due to receptor competition with these antibodies for epitopes in G (11, 21). Similarly, we found here that MAb26 binding to HeV G was significantly reduced (61%) in the presence of soluble receptor (100 nM ephrin B2) compared to the level of binding in the absence of receptor (0 nM ephrin B2; shown by dotted line in Fig. 6C). All HeV G N-glycan mutants showed decreased MAb26 binding upon receptor engagement, similar to the results for WT HeV G, with the decreases ranging from 51 to 70% (Fig. 6C). These results indicate that the removal of HeV G N-glycans does not significantly affect

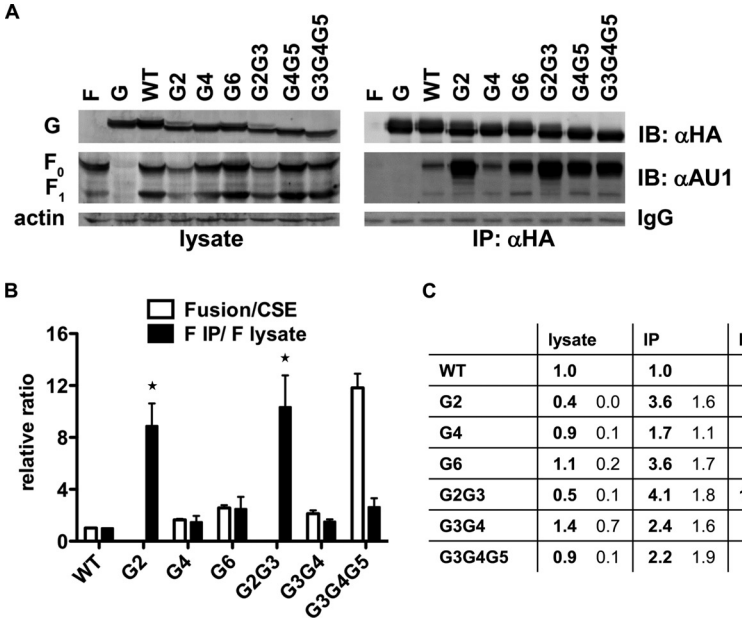

C

	lysate		IP		IP/lysate	
WT	**1.0**		**1.0**		**1.0**	
G2	**0.4**	0.0	**3.6**	1.6	**8.9**	1.7
G4	**0.9**	0.1	**1.7**	1.1	**1.5**	0.5
G6	**1.1**	0.2	**3.6**	1.7	**2.5**	0.9
G2G3	**0.5**	0.1	**4.1**	1.8	**10.3**	2.4
G3G4	**1.4**	0.7	**2.4**	1.6	**1.5**	0.2
G3G4G5	**0.9**	0.1	**2.2**	1.9	**2.6**	0.7

FIG 5 HeV G N-glycan mutants modulate G-F interactions. (A) The G-F interactions of WT HeV F and WT or mutant HeV G were determined by immunoprecipitating HeV G from transfected 293T cells using μMACS anti-HA antibody-coated MicroBeads. Total cell lysates (lysate) and coimmunoprecipitated proteins (IP: αHA) were separated by 10% SDS-PAGE and immunoblotted with HeV F (IB: αAU1)- and HeV G (IB: αHA)-specific antibodies. Cell lysates from cells transfected with F or G only served as the respective negative or positive controls. Actin was detected as an internal loading control for lysate samples, and IgG (light chain) for immunoprecipitated proteins (IP). (B) Fusion indices described in Table 1 are plotted next to the avidities of G-F interactions, which were measured as the ratio of the amount of coimmunoprecipitated F (IP) to the amount of total F (F_0 and F_1) present in the cell lysate (F IP/F lysate). The relative ratios were measured by normalizing the values for mutant HeV G to those for WT HeV G (set to 1). The individual amounts were measured by densitometry using ImageLab software. The data represent the average results ± SEM from three independent experiments. (C) Individual data (lysate versus IP) used to calculate the avidities of G-F interactions are shown.

receptor-induced conformational change (step 1) at the membrane distal portion of the HeV G head.

The step 2 conformational change takes place at the base of the NiV/HeV G head and precedes F triggering. Ephrin B2 binding induces a roughly 2-fold increase in MAb45 binding to WT NiV G (11, 21, 28, 29). Ephrin B2 binding to WT HeV G also resulted in a roughly 2-fold increase in MAb45 binding (Fig. 6C). Therefore, our combined results showed for the first time that HeV G undergoes receptor-induced conformational changes similarly to NiV G. Moreover, most N-glycan mutants showed an increase in MAb45 binding, ranging from 1.5- to 3.2-fold. In contrast, the G2 and G2G3 stalk mutants showed a decreased (~ 40%) or roughly equal level of MAb45 binding, respectively, upon ephrin B2 receptor binding to HeV G (Fig. 6B). These results suggest that the G2 N-glycan in the stalk region of HeV G (residue 159) is crucial for the step 2 conformational change to occur.

HeV G N-glycans protect virions from neutralizing antibodies. For a range of viruses, it has been shown that glycan shields can protect the viruses from antibody neutralization (14, 20, 30–34). We asked whether the removal of N-glycans in HeV G would lead to enhanced virus neutralization by anti-HeV specific rabbit polyclonal antiserum 837. We analyzed the antibody neutralization of HeV/VSV-rLuc virions pseudotyped with WT HeV F and WT or mutant HeV G (Fig. 7A and B, respectively). Overall, HeV/VSV-rLuc virion neutralization was more efficient when two or more N-glycans were removed than when single N-glycans were removed (Fig. 7A and B, respectively). Statistical analysis (Student's *t* test) of data obtained for the 10^{-4} antiserum dilution revealed that the neutralization of the G5, G3G5, G4G5, G6G7, and G3G4G5 mutants was statistically different from the neutralization of WT HeV G ($P < 0.05$). The neutralization of the G6 ($P = 0.060$), G7 (0.050), G3G4 ($P = 0.054$), and G4G7 (0 = 0.058) mutants just missed borderline statistical significance. The G3 and G4 single mutants were neutralized similarly to wild-type HeV G, whereas the 50% inhibitory concentration (IC_{50}) of the G5 mutant was reduced by 0.5 log. The G4G5 and G3G4G5 multiple N-glycan mutants were neutralized at a roughly 1-log-lower IC_{50} than wild-type HeV G. No significant difference could be observed between G4G5 and G3G4G5 mutant virions, supporting the notion that the G3 single mutant neither protects from nor contributes to antibody neutralization. Overall, these data confirm that N-glycans in HeV G provide Hendra virus with a shield to evade neutralizing antibodies; however, the degree of evasion varies among N-glycans, with the HeV G5 N-glycan having a strong role in shielding against antibody neutralization. Our results indicate that N-glycans in HeV G shield against antibody neutralization and that individual N-glycans have distinct effects on antibody neutralization.

DISCUSSION

In the last decade, there has been an increased interest in understanding the importance of glycosylation (N- and O-glycosylation) of viral glycoproteins, as glycans have been shown to affect, among other functions, protein folding, the induction of interferon, and regulation of antiviral responses by shielding the virus from neutralizing antibodies (14, 20, 30–35). Similar observations have been made for some paramyxoviruses, where N-glycans have been shown to modulate protein conformation, protein expression, and membrane fusion (14, 20, 36, 37).

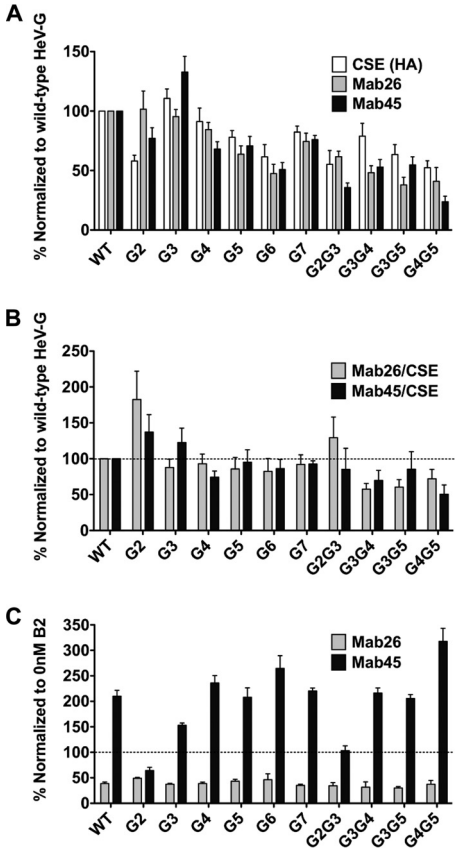

FIG 6 HeV G stalk N-glycan mutants modulate receptor-induced conformational changes differently than WT HeV G. (A) Ephrin B2-deficient PK13 cells were transfected with WT or mutant HeV G to assess cell surface expression (CSE) and MAb26 and MAb45 binding in the absence of receptor by flow cytometry. The CSE, MAb26, and MAb45 binding levels of the HeV G N-glycan mutants were normalized to the corresponding levels obtained for WT HeV G (set to 100%). (B) The ratios of MAb26 or MAb45 binding levels to CSE were determined and normalized to that of WT HeV G (set to 100%; dotted line). (C) MAb26 and MAb45 binding levels to HeV G N-glycan mutants were determined in PK13 cells in the absence (0 nM) and presence (100 nM) of soluble ephrin B2. Binding levels in the presence of ephrin B2 were normalized to binding levels in the absence of ephrin B2 (set to 100%; dotted line). The data represent the average results ± SEM from at least three independent experiments.

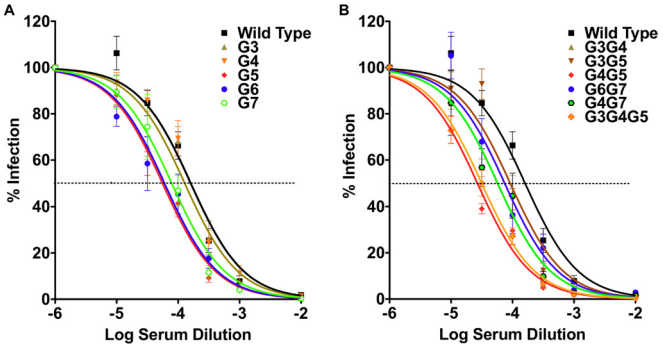

FIG 7 HeV G N-glycans protect HeV against neutralizing antibodies. Pseudotyped HeV/VSV-rLuc virions with incorporated WT HeV F and WT or mutant HeV G were neutralized with various concentrations of HeV G-specific rabbit polyclonal antiserum 837 prior to infecting Vero cells. Infected Vero cells were measured for relative light units (RLU) 18 to 24 h postinfection. Single (A) and multiple (B) HeV G N-glycan mutants were tested. Logarithms of the dilutions of 1 mg/ml serum stocks are shown. The average results ± SEM from at least six independent experiments with triplicate wells per experiment are shown. The 50% inhibitory concentration (IC_{50}) is represented by a dotted line.

Our study was meticulously designed to understand the functions of N-glycans in the HeV attachment protein G (HeV G). We found that six of eight potential N-glycosylation sites are glycosylated (G2 to G7) in HeV G (Fig. 1A and B). Thus, the actual N-glycan sites occupied are identical to those we previously reported for NiV G (14). However, with regard to HeV G, there are differing reports about the existence of N-glycosylation at the HeV G5 site (residue 417), which may be due to the different expression systems used (14, 38–41). Interestingly, it appears that the removal of multiple N-glycans has relatively more severe effects on CSE for HeV G (down to 0 to 2% CSE for triple mutants) (Fig. 2C) than for NiV G (10 to 20% CSE for triple mutants [14]).

G2 is located within the stalk region, while sites G3 to G7 are positioned in the globular head domain on surface-exposed loops (Fig. 1B) (15, 41). Here, we demonstrated that N-glycosylation of HeV G is important for overall protein stability (as demonstrated by reduced steady-state protein levels, especially when multiple N-glycans were removed), protein transport to the cell surface, cell-cell fusion, viral entry, conformation (i.e., oligomerization and/or MAb reactivity) and G-F interactions. Interestingly, the removal of an N-glycan at position G2 (residue 159) in the stalk domain of HeV G affected all of these functions, similarly to what has previously been described for NiV G2 (14, 27). This indicates that glycosylation at the G2 site is of crucial importance to the life cycle of both HeV and NiV.

N-glycans in HeV and NiV G had qualitatively similar but quantitatively different contributions to cell-cell fusion, as described in Table 1. In summary, it appears that the removal of G3 and G4 N-glycans leads to higher fusion indices for HeV G (FIs of 1.29 and 1.64, respectively) than for NiV G (FIs of 0.86 and 1.11, respectively). This effect was even more pronounced in the G3G4G5 mutant (FI of 11.81 for HeV and 4.49 for NiV) (Table 1). In contrast, the removal of G6 and G7 N-glycans yielded higher fusion indices in NiV G (FIs of 6.4 and 1.6, respectively) than for HeV G (FIs of 2.6 and 1.0, respectively). Overall, these data suggest that the G3 and G4 N-glycans suppress cell-cell fusion in WT HeV, while the G7 N-glycan suppresses cell-cell fusion in WT NiV. The G6 N-glycan, however, suppresses cell-cell fusion in both HeV and NiV, although more severely in NiV. These data agree with the notion that HeV and NiV do not modulate membrane fusion in identical ways, as was shown recently (42). Interestingly, in NiV G, some triple N-glycan mutants (G4G5G6 and G4G6G7 mutants) were still able to induce fusion (FIs of 5.9 and 6.7, respectively), whereas in the case of HeV G, these mutants were close to fusion dead, probably due to their extremely low CSE levels (FIs could not be determined) (Table 1). Whether the differential effects of specific N-glycans in modulating membrane fusion are due to differences in the types of N-glycans added to equivalent N-glycosylation sites in HeV versus NiV G remains to be determined.

Virus-cell and cell-cell membrane fusion are mediated by the viral fusion protein F, which for HeV and NiV requires the attachment protein G. In order to become fusogenically active, a fusogenically inactive F_0 protein undergoes endocytic recycling and proteolytic processing into the disulfide-linked F_1 and F_2 forms by the cellular protease cathepsin L (43). Since N-glycan removal in HeV G affected fusion mostly positively, but sometimes negatively

(for the G2 and G2G3 mutants), we analyzed whether the G-F interactions and F processing were affected by N-glycan removal. Generally, greater numbers of N-glycans removed correlated with higher fusion levels (considering the protein cell surface expression levels) (Fig. 1 and 2).

Interestingly, for the fusion-dead G2 and G2G3 mutants, we observed an inverse relationship between fusion and G-F binding avidity (Fig. 5B). In addition, these G mutants also reduced the total amount of F protein in the cells by about 2.5-fold, suggesting that the G2 N-glycan may have important effects on F protein stability, e.g., by affecting F protein turnover (Fig. 5A, left). One potential explanation for these observations is that HeV G in the absence of the G2 N-glycan has a stronger affinity to the inactive precursor F_0 and is trapping F_0 on the cell surface. This may result in delayed recycling and a longer retention of F_0 in the endosomal compartment, resulting in reduced levels of cleaved F_1 being available to bind to G and execute cell-cell fusion. In addition, the G2 and G2G3 stalk mutants all appeared to have less processed F_1 incorporated into virions than F_0 (32% and 26%, respectively) compared to the results for WT HeV G (41 to 49%) (Fig. 3B and 4B). The viral incorporation levels are likely a direct reflection of the glycoprotein levels present on the cell surface, as paramyxoviruses bud from the cell surface. We previously observed an inverse correlation between fusion and F binding while analyzing hypofusogenic NiV F N-glycan mutants (20). The present study is the first to report that this inverse relationship also holds true for hypofusogenic G N-glycan mutants.

The viral entry levels generally correlated with the cell-cell fusion levels for each mutant analyzed. For example, the G2 stalk mutant showed neither cell-cell fusion nor viral entry, and the G3G4G5 cell-cell hyperfusogenic mutant also showed enhanced viral entry, considering the relative reduction in viral glycoprotein incorporation compared to the results for WT G (Fig. 1 to 4). Interestingly, the predicted but not occupied G1 N-glycan site (located in the stalk) showed an opposite pattern, with a cell-cell hypofusogenic phenotype but a viral entry level similar to or higher than that of WT HeV G. Both stalk mutants showed similar phenotypes in NiV G and, thus, are likely valuable tools to further understand the role of the G stalk in viral entry and cell-cell fusion and the apparent mechanistic differences between these two important events in the viral life cycle. It is also noteworthy that the pseudotyped viruses did not incorporate any appreciable amounts of monomers for either the wild-type or mutant HeV G proteins (Fig. 3B and 4B). To our knowledge, this is the first time that the selective HeV incorporation of higher oligomers has been reported. Whether this is also true for NiV or other paramyxoviruses remains to be determined.

We previously reported that NiV G undergoes receptor-induced conformational changes that can be measured with conformational antibodies (11). These antibodies can detect changes in G conformations in the absence versus the presence of soluble receptor ephrin B2. Here, we first showed that HeV G undergoes receptor-induced conformational changes similar to those seen for NiV G (Fig. 6). In addition, all N-glycan mutants were able to undergo the conformational step 1 (MAb26) change, while most mutants were able to undergo the conformational step 2 (MAb45) change, with the exception of the HeV G2 and G2G3 mutants. Additionally, in the pre-receptor binding state, most single N-glycan mutants bound more or less equally well to MAb26 and MAb45, with the exception of the G2 N-glycan mutant, which exhibited enhanced binding to both antibodies (Fig. 6B). In combination, our data suggest that the G2 and G2G3 mutants proteins are present in a conformation distinct from that of WT HeV G, and we speculate that this conformation corresponds to an intermediate one between steps 1 and 2 post-receptor binding. This notion is consistent with the status of both conformational antibody binding and oligomerization being altered for these mutant proteins.

It is also possible that a carbohydrate at the G2 position causes steric hindrance for MAb45 binding, since its epitope binding site is located at the base of the head (residue 177 to 194) in close proximity to the G2 N-glycan position (residue 159) and, hence, upon the removal of the G2 carbohydrate, enhanced MAb45 binding is observed. However, this explanation is not possible for MAb26, since MAb26 binding occurs at the top of the HeV G head (residue 371 to 392), close to the receptor binding site (11, 21). Therefore, we favor the notion that the G2 mutant is in a different conformation than WT HeV G.

We also observed a roughly 50% increase in MAb45 binding for the double mutant G4G5 upon receptor engagement compared to that of WT HeV G (Fig. 6C), suggesting that the removal of certain N-linked glycans may enhance conformational changes in a viral protein. In other words, certain N-glycans can sterically delay large conformational changes in a protein, which has been documented before for a nonviral protein (Fig. 6C) (44). We also noticed that the receptor-induced conformational change detected by MAb45 appears to be somewhat suppressed in the G3 mutant (Fig. 6C), which may be due to a proportion of the G3 proteins being in a post-receptor binding conformation or to all the G3 proteins being in an intermediate conformation between the pre- and postfusion conformations (Fig. 6B). However, the lower level of conformational change in the G3 mutant appears to be sufficient for both cell-cell fusion and viral entry to occur (Fig. 1C and 3A).

When taking all our G2 mutant results into account, it is also possible that MAb45 preferentially binds to the tetrameric state of HeV G, which is the preferred oligomeric state of the HeV G2 N-glycan mutant on the virus or cell surface (Fig. 3B). We recently observed a similar aberrant oligomerization pattern for a different type of NiV G2 N-glycan mutant (Asn to Ala), which showed reduced levels of dimeric G, suggesting that the conserved stalk regions in HeV and NiV share similar functions (27). This was not the case for the HeV G G3 to G7 N-glycan mutants, which approached wild-type levels of both dimeric and tetrameric G (Fig. 3B). However, we do not favor this notion that MAb45 preferably binds tetramers. Evidently, studies of several paramyxoviruses, including NiV, measles virus, Newcastle disease virus, and parainfluenza virus 5, have suggested that tetramer dissociation is important during H or G triggering (reviewed in reference 45), and our prior work showed that enhancement of MAb45 binding correlates with tetramer dissociation (21). From a structural perspective, we believe that the removal of the G2 N-glycan increases the interaction between the subunit stalk domains, which causes an increase in tetrameric stability, but tetramer dissociation is likely important for fusion promotion.

Viruses have evolved to display their own carbohydrate compositions to evade or interfere with host glycan-based interactions and immune functions. The N-linked glycoproteins of the highly pathogenic Ebola virus (GP), human immunodeficiency virus (HIV) (gp120), and hepatitis C virus (E1 and E2), for example, contain more high-mannose than complex carbohydrate structures (35). In contrast, previous spectrometric analyses of carbohydrate moieties present in HeV and NiV G revealed that the

N-glycans are largely the complex type, with only negligible amounts of high-mannose-type carbohydrates (24, 38). Since HeV and NiV G appear to have similar carbohydrate type compositions, their N-glycans may possibly differ in their variability or in their branching patterns, which in turn may alter virus infectivity. For example, 29 different glycan structures were identified for soluble HeV G alone (24). An indication that different glycan structures may exist in HeV G and NiV G is the fact that the neutralizing epitopes show very little conservation between HeV G and NiV G, even though these viruses share strong serological cross-reactivity (46–48). Understanding the role of specific N-glycans in protecting the virus from neutralizing antibodies may help in HeV vaccine development.

We recently reported that N-glycans in NiV G protect virions from antibody neutralization and have important roles in viral entry and cell-cell fusion (14). Despite high amino acid identity, some reports suggest a level of inherent differences in the structure and/or function of NiV and HeV G glycoproteins (48, 49). For example, NiV G binds monoclonal antibody m102.4 better than HeV G, despite m102.4 having been selected against sG_{HeV} (49). We performed an antibody neutralization assay on WT and mutant HeV G virions, and the results indicate that most N-glycans in HeV G had some role in protection, especially in combination with other N-glycans (Fig. 7). However, the HeV G N-glycan at position G5 (residue 417) in particular appeared to have a major role in protection from antibody neutralization, possibly by preventing the complete exposure of a major neutralizing epitope site. From our results, we predict that the antigenicity of HeV G may be enhanced by selective deglycosylation, a technique that has been successfully used for other viruses, such as feline immunodeficiency virus (FIV) and HIV (50, 51).

Selective deglycosylation at the G2 site may additionally be advantageous for improving vaccine design, since the G2 mutant virions preferentially incorporate a more stable tetrameric state of G, possibly present in an intermediate fusion conformation. Oligomeric proteins are generally known to induce a more robust immune response than monomeric constructs (52). In addition, the carbohydrate removal at the G2 position likely leads to a replication-deficient henipavirus and, therefore, might make it an attractive vaccine candidate. However, whether this holds true *in vivo* remains to be determined.

Taken together, our results showed important functions in modulating G cell surface expression, induction of membrane fusion, viral entry, interactions with F, and shielding against antibody neutralization that are specific to HeV G N-glycans. We also noted qualitative commonalities and quantitative differences between specific N-glycan functions in HeV and NiV. Elucidating the role(s) of such commonalities and differences will likely contribute to understanding the pathobiology of these viruses and the requirements for optimal vaccine development.

ACKNOWLEDGMENT

This study was supported by NIH/NIAID grant AI109022 to H.C.A.

REFERENCES

1. **Aguilar HC, Lee B.** 2011. Emerging paramyxoviruses: molecular mechanisms and antiviral strategies. Expert Rev Mol Med **13:**e6. http://dx.doi.org/10.1017/S1462399410001754.
2. **Marsh GA, de Jong C, Barr JA, Tachedjian M, Smith C, Middleton D, Yu M, Todd S, Foord AJ, Haring V, Payne J, Robinson R, Broz I, Crameri G, Field HE, Wang LF.** 2012. Cedar virus: a novel Henipavirus isolated from Australian bats. PLoS Pathog **8:**e1002836. http://dx.doi.org/10.1371/journal.ppat.1002836.
3. **Geisbert TW, Feldmann H, Broder CC.** 2012. Animal challenge models of henipavirus infection and pathogenesis. Curr Top Microbiol Immunol **359:**153–177. http://dx.doi.org/10.1007/82_2012_208.
4. **Middleton D, Pallister J, Klein R, Feng YR, Haining J, Arkinstall R, Frazer L, Huang JA, Edwards N, Wareing M, Elhay M, Hashmi Z, Bingham J, Yamada M, Johnson D, White J, Foord A, Heine HG, Marsh GA, Broder CC, Wang LF.** 2014. Hendra virus vaccine, a one health approach to protecting horse, human, and environmental health. Emerg Infect Dis **20:**372–379. http://dx.doi.org/10.3201/eid2003.131159.
5. **NSW Department of Primary Industries.** 29 August 2014. reviewed. NSW Department of Primary Industries, agriculture: Hendra virus, current situation July 2014. http://www.dpi.nsw.gov.au/agriculture/livestock/horses/health/general/hendra-virus.
6. **Hazelton B, Ba Alawi F, Kok J, Dwyer DE.** 2013. Hendra virus: a one health tale of flying foxes, horses and humans. Future Microbiol **8:**461–474. http://dx.doi.org/10.2217/fmb.13.19.
7. **Broder CC, Xu K, Nikolov DB, Zhu Z, Dimitrov DS, Middleton D, Pallister J, Geisbert TW, Bossart KN, Wang LF.** 2013. A treatment for and vaccine against the deadly Hendra and Nipah viruses. Antiviral Res **100:**8–13. http://dx.doi.org/10.1016/j.antiviral.2013.06.012.
8. **Geisbert TW, Mire CE, Geisbert JB, Chan YP, Agans KN, Feldmann F, Fenton KA, Zhu Z, Dimitrov DS, Scott DP, Bossart KN, Feldmann H, Broder CC.** 2014. Therapeutic treatment of Nipah virus infection in nonhuman primates with a neutralizing human monoclonal antibody. Sci Transl Med **6:**242ra82. http://dx.doi.org/10.1126/scitranslmed.3008929.
9. **Bossart KN, Fusco DL, Broder CC.** 2013. Paramyxovirus entry. Adv Exp Med Biol **790:**95–127. http://dx.doi.org/10.1007/978-1-4614-7651-1_6.
10. **Lamb RA, Paterson RG, Jardetzky TS.** 2006. Paramyxovirus membrane fusion: lessons from the F and HN atomic structures. Virology **344:**30–37. http://dx.doi.org/10.1016/j.virol.2005.09.007.
11. **Liu Q, Stone JA, Bradel-Tretheway B, Dabundo J, Benavides Montano JA, Santos-Montanez J, Biering SB, Nicola AV, Iorio RM, Lu X, Aguilar HC.** 2013. Unraveling a three-step spatiotemporal mechanism of triggering of receptor-induced Nipah virus fusion and cell entry. PLoS Pathog **9:**e1003770. http://dx.doi.org/10.1371/journal.ppat.1003770.
12. **Bishop KA, Hickey AC, Khetawat D, Patch JR, Bossart KN, Zhu Z, Wang LF, Dimitrov DS, Broder CC.** 2008. Residues in the stalk domain of the Hendra virus G glycoprotein modulate conformational changes associated with receptor binding. J Virol **82:**11398–11409. http://dx.doi.org/10.1128/JVI.02654-07.
13. **Maar D, Harmon B, Chu D, Schulz B, Aguilar HC, Lee B, Negrete OA.** 2012. Cysteines in the stalk of the Nipah virus G glycoprotein are located in a distinct subdomain critical for fusion activation. J Virol **86:**6632–6642. http://dx.doi.org/10.1128/JVI.00076-12.
14. **Biering SB, Huang A, Vu AT, Robinson LR, Bradel-Tretheway B, Choi E, Lee B, Aguilar HC.** 2012. N-glycans on the Nipah virus attachment glycoprotein modulate fusion and viral entry as they protect against antibody neutralization. J Virol **86:**11991–12002. http://dx.doi.org/10.1128/JVI.01304-12.
15. **Guillaume V, Aslan H, Ainouze M, Guerbois M, Wild TF, Buckland R, Langedijk JP.** 2006. Evidence of a potential receptor-binding site on the Nipah virus G protein (NiV-G): identification of globular head residues with a role in fusion promotion and their localization on an NiV-G structural model. J Virol **80:**7546–7554. http://dx.doi.org/10.1128/JVI.00190-06.
16. **Negrete OA, Chu D, Aguilar HC, Lee B.** 2007. Single amino acid changes in the Nipah and Hendra virus attachment glycoproteins distinguish ephrinB2 from ephrinB3 usage. J Virol **81:**10804–10814. http://dx.doi.org/10.1128/JVI.00999-07.
17. **Negrete OA, Levroney EL, Aguilar HC, Bertolotti-Ciarlet A, Nazarian R, Tajyar S, Lee B.** 2005. EphrinB2 is the entry receptor for Nipah virus, an emergent deadly paramyxovirus. Nature **436:**401–405. http://dx.doi.org/10.1038/nature03838.
18. **Negrete OA, Wolf MC, Aguilar HC, Enterlein S, Wang W, Muhlberger E, Su SV, Bertolotti-Ciarlet A, Flick R, Lee B.** 2006. Two key residues in ephrinB3 are critical for its use as an alternative receptor for Nipah virus. PLoS Pathog **2:**e7. http://dx.doi.org/10.1371/journal.ppat.0020007.
19. **Levroney EL, Aguilar HC, Fulcher JA, Kohatsu L, Pace KE, Pang M, Gurney KB, Baum LG, Lee B.** 2005. Novel innate immune functions for galectin-1: galectin-1 inhibits cell fusion by Nipah virus envelope glycoproteins and augments dendritic cell secretion of proinflammatory cytokines. J Immunol **175:**413–420. http://dx.doi.org/10.4049/jimmunol.175.1.413.

20. **Aguilar HC, Matreyek KA, Filone CM, Hashimi ST, Levroney EL, Negrete OA, Bertolotti-Ciarlet A, Choi DY, McHardy I, Fulcher JA, Su SV, Wolf MC, Kohatsu L, Baum LG, Lee B.** 2006. N-glycans on Nipah virus fusion protein protect against neutralization but reduce membrane fusion and viral entry. J Virol **80:**4878–4889. http://dx.doi.org/10.1128/JVI.80.10.4878-4889.2006.
21. **Aguilar HC, Ataman ZA, Aspericueta V, Fang AQ, Stroud M, Negrete OA, Kammerer RA, Lee B.** 2009. A novel receptor-induced activation site in the Nipah virus attachment glycoprotein (G) involved in triggering the fusion glycoprotein (F). J Biol Chem **284:**1628–1635. http://dx.doi.org/10.1074/jbc.M807469200.
22. **Aguilar HC, Matreyek KA, Choi DY, Filone CM, Young S, Lee B.** 2007. Polybasic KKR motif in the cytoplasmic tail of Nipah virus fusion protein modulates membrane fusion by inside-out signaling. J Virol **81:**4520–4532. http://dx.doi.org/10.1128/JVI.02205-06.
23. **Whitman SD, Dutch RE.** 2007. Surface density of the Hendra G protein modulates Hendra F protein-promoted membrane fusion: role for Hendra G protein trafficking and degradation. Virology **363:**419–429. http://dx.doi.org/10.1016/j.virol.2007.01.029.
24. **Colgrave ML, Snelling HJ, Shiell BJ, Feng YR, Chan YP, Bossart KN, Xu K, Nikolov DB, Broder CC, Michalski WP.** 2012. Site occupancy and glycan compositional analysis of two soluble recombinant forms of the attachment glycoprotein of Hendra virus. Glycobiology **22:**572–584. http://dx.doi.org/10.1093/glycob/cwr180.
25. **Xu K, Chan YP, Rajashankar KR, Khetawat D, Yan L, Kolev MV, Broder CC, Nikolov DB.** 2012. New insights into the Hendra virus attachment and entry process from structures of the virus G glycoprotein and its complex with Ephrin-B2. PLoS One **7:**e48742. http://dx.doi.org/10.1371/journal.pone.0048742.
26. **White JM, Delos SE, Brecher M, Schornberg K.** 2008. Structures and mechanisms of viral membrane fusion proteins: multiple variations on a common theme. Crit Rev Biochem Mol Biol **43:**189–219. http://dx.doi.org/10.1080/10409230802058320.
27. **Liu Q, Bradel-Tretheway B, Monreal AI, Saludes JP, Lu X, Nicola AV, Aguilar HC.** 2015. Nipah virus attachment glycoprotein stalk C-terminal region links receptor binding to fusion triggering. J Virol **89:**1838–1850. http://dx.doi.org/10.1128/JVI.02277-14.
28. **Zhu Q, Biering SB, Mirza AM, Grasseschi BA, Mahon PJ, Lee B, Aguilar HC, Iorio RM.** 2013. Individual N-glycans added at intervals along the stalk of the Nipah virus G protein prevent fusion but do not block the interaction with the homologous F protein. J Virol **87:**3119–3129. http://dx.doi.org/10.1128/JVI.03084-12.
29. **Mirza AM, Aguilar HC, Zhu Q, Mahon PJ, Rota PA, Lee B, Iorio RM.** 2011. Triggering of the Newcastle disease virus fusion protein by a chimeric attachment protein that binds to Nipah virus receptors. J Biol Chem **286:**17851–17860. http://dx.doi.org/10.1074/jbc.M111.233965.
30. **Kropff B, Burkhardt C, Schott J, Nentwich J, Fisch T, Britt W, Mach M.** 2012. Glycoprotein N of human cytomegalovirus protects the virus from neutralizing antibodies. PLoS Pathog **8:**e1002999. http://dx.doi.org/10.1371/journal.ppat.1002999.
31. **Lennemann NJ, Rhein BA, Ndungo E, Chandran K, Qiu X, Maury W.** 2014. Comprehensive functional analysis of N-linked glycans on Ebola virus GP1. mBio **5**(1):e00862-13. http://dx.doi.org/10.1128/mBio.00862-13.
32. **Julithe R, Abou Jaoude G, Sureau C.** 2014. Modification of the hepatitis B virus envelope protein glycosylation pattern interferes with secretion of viral particles, infectivity, and susceptibility to neutralizing antibodies. J Virol **88:**9049–9059. http://dx.doi.org/10.1128/JVI.01161-14.
33. **de Haan CA, de Wit M, Kuo L, Montalto-Morrison C, Haagmans BL, Weiss SR, Masters PS, Rottier PJ.** 2003. The glycosylation status of the murine hepatitis coronavirus M protein affects the interferogenic capacity of the virus in vitro and its ability to replicate in the liver but not the brain. Virology **312:**395–406. http://dx.doi.org/10.1016/S0042-6822(03)00235-6.
34. **Laude H, Gelfi J, Lavenant L, Charley B.** 1992. Single amino acid changes in the viral glycoprotein M affect induction of alpha interferon by the coronavirus transmissible gastroenteritis virus. J Virol **66:**743–749.
35. **Vigerust DJ, Shepherd VL.** 2007. Virus glycosylation: role in virulence and immune interactions. Trends Microbiol **15:**211–218. http://dx.doi.org/10.1016/j.tim.2007.03.003.
36. **McGinnes L, Sergel T, Reitter J, Morrison T.** 2001. Carbohydrate modifications of the NDV fusion protein heptad repeat domains influence maturation and fusion activity. Virology **283:**332–342. http://dx.doi.org/10.1006/viro.2001.0899.
37. **Sawatsky B, von Messling V.** 2010. Canine distemper viruses expressing a hemagglutinin without N-glycans lose virulence but retain immunosuppression. J Virol **84:**2753–2761. http://dx.doi.org/10.1128/JVI.01813-09.
38. **Bowden TA, Crispin M, Harvey DJ, Aricescu AR, Grimes JM, Jones EY, Stuart DI.** 2008. Crystal structure and carbohydrate analysis of Nipah virus attachment glycoprotein: a template for antiviral and vaccine design. J Virol **82:**11628–11636. http://dx.doi.org/10.1128/JVI.01344-08.
39. **Bowden TA, Crispin M, Harvey DJ, Jones EY, Stuart DI.** 2010. Dimeric architecture of the Hendra virus attachment glycoprotein: evidence for a conserved mode of assembly. J Virol **84:**6208–6217. http://dx.doi.org/10.1128/JVI.00317-10.
40. **Xu K, Rajashankar KR, Chan YP, Himanen JP, Broder CC, Nikolov DB.** 2008. Host cell recognition by the henipaviruses: crystal structures of the Nipah G attachment glycoprotein and its complex with ephrin-B3. Proc Natl Acad Sci U S A **105:**9953–9958. http://dx.doi.org/10.1073/pnas.0804797105.
41. **Xu K, Rockx B, Xie Y, DeBuysscher BL, Fusco DL, Zhu Z, Chan YP, Xu Y, Luu T, Cer RZ, Feldmann H, Mokashi V, Dimitrov DS, Bishop-Lilly KA, Broder CC, Nikolov DB.** 2013. Crystal structure of the Hendra virus attachment G glycoprotein bound to a potent cross-reactive neutralizing human monoclonal antibody. PLoS Pathog **9:**e1003684. http://dx.doi.org/10.1371/journal.ppat.1003684.
42. **Yun T, Park A, Hill TE, Pernet O, Beaty SM, Juelich TL, Smith JK, Zhang LH, Wang YE, Vigant F, Gao JL, Wu P, Lee B, Freiberg AN.** 2015. Efficient reverse genetics reveals genetic determinants of budding and fusogenic differences between Nipah and Hendra viruses and enables real-time monitoring of viral spread in small animal models of henipavirus infection. J Virol **89:**1242–1253. http://dx.doi.org/10.1128/JVI.02583-14.
43. **Popa A, Carter JR, Smith SE, Hellman L, Fried MG, Dutch RE.** 2012. Residues in the Hendra virus fusion protein transmembrane domain are critical for endocytic recycling. J Virol **86:**3014–3026. http://dx.doi.org/10.1128/JVI.05826-11.
44. **Bager R, Johansen JS, Jensen JK, Stensballe A, Jendroszek A, Buxbom L, Sorensen HP, Andreasen PA.** 2013. Protein conformational change delayed by steric hindrance from an N-linked glycan. J Mol Biol **425:**2867–2877. http://dx.doi.org/10.1016/j.jmb.2013.05.007.
45. **Jardetzky TS, Lamb RA.** 2014. Activation of paramyxovirus membrane fusion and virus entry. Curr Opin Virol **5:**24–33. http://dx.doi.org/10.1016/j.coviro.2014.01.005.
46. **Chua KB, Bellini WJ, Rota PA, Harcourt BH, Tamin A, Lam SK, Ksiazek TG, Rollin PE, Zaki SR, Shieh W, Goldsmith CS, Gubler DJ, Roehrig JT, Eaton B, Gould AR, Olson J, Field H, Daniels P, Ling AE, Peters CJ, Anderson LJ, Mahy BW.** 2000. Nipah virus: a recently emergent deadly paramyxovirus. Science **288:**1432–1435. http://dx.doi.org/10.1126/science.288.5470.1432.
47. **Harcourt BH, Tamin A, Ksiazek TG, Rollin PE, Anderson LJ, Bellini WJ, Rota PA.** 2000. Molecular characterization of Nipah virus, a newly emergent paramyxovirus. Virology **271:**334–349. http://dx.doi.org/10.1006/viro.2000.0340.
48. **White JR, Boyd V, Crameri GS, Duch CJ, van Laar RK, Wang LF, Eaton BT.** 2005. Location of, immunogenicity of and relationships between neutralization epitopes on the attachment protein (G) of Hendra virus. J Gen Virol **86:**2839–2848. http://dx.doi.org/10.1099/vir.0.81218-0.
49. **Zhu Z, Bossart KN, Bishop KA, Crameri G, Dimitrov AS, McEachern JA, Feng Y, Middleton D, Wang LF, Broder CC, Dimitrov DS.** 2008. Exceptionally potent cross-reactive neutralization of Nipah and Hendra viruses by a human monoclonal antibody. J Infect Dis **197:**846–853. http://dx.doi.org/10.1086/528801.
50. **Willett BJ, McMonagle EL, Logan N, Samman A, Hosie MJ.** 2008. A single site for N-linked glycosylation in the envelope glycoprotein of feline immunodeficiency virus modulates the virus-receptor interaction. Retrovirology **5:**77. http://dx.doi.org/10.1186/1742-4690-5-77.
51. **Ma BJ, Alam SM, Go EP, Lu X, Desaire H, Tomaras GD, Bowman C, Sutherland LL, Scearce RM, Santra S, Letvin NL, Kepler TB, Liao HX, Haynes BF.** 2011. Envelope deglycosylation enhances antigenicity of HIV-1 gp41 epitopes for both broad neutralizing antibodies and their unmutated ancestor antibodies. PLoS Pathog **7:**e1002200. http://dx.doi.org/10.1371/journal.ppat.1002200.
52. **Bachmann MF, Zinkernagel RM.** 1997. Neutralizing antiviral B cell responses. Annu Rev Immunol **15:**235–270. http://dx.doi.org/10.1146/annurev.immunol.15.1.235.